BUILD SIMUL (2023) 16: 51–67
https://doi.org/10.1007/s12273-022-0921-0

Multi-objective optimization of equipment capacity and heating network design for a centralized solar district heating system

Yanfeng Liu[1,2], Ting Mu[1,2], Xi Luo[1,2] (✉)

1. School of Building Services Science and Engineering, Xi'an University of Architecture and Technology, Xi'an 710055, China
2. State Key Laboratory of Green Building in Western China, Xi'an 710055, China

Abstract

Northwest China has abundant solar energy resources and a large demand for winter heating. Using solar energy for centralized heating is a clean and effective way to solve local heating problems. While present studies usually decoupled solar heating stations and the heating network in the optimization design of centralized solar heating systems, this study developed a joint multi-objective optimization model for the equipment capacity and the diameters of the heating network pipes of a centralized solar district heating system, using minimum total life cycle cost and CO_2 emission of the system as the optimization objectives. Three typical cities in northwest China with different solar resource conditions (Lhasa, Xining, and Xi'an) were selected as cases for analysis. According to the results, the solar heating system designed using the method proposed in this study presents lower economic cost and higher environmental protection in comparison to separately optimizing the design of the solar heating station and the heating network. Furthermore, the solar fraction of the optimal systems are 90%, 70%, and 31% for Lhasa, Xining, and Xi'an, and the minimum water supply temperatures are 55 °C, 50 °C, and 65 °C for an optimal economy and 55 °C, 45 °C, and 45 °C for optimal environmental protection, respectively. It was also established that the solar collector price has a greater impact on the equipment capacity of the solar heating station than the gas boiler price.

Keywords

solar energy;
solar energy system;
district heating;
optimization design;
genetic algorithm

Article History

Received: 22 April 2022
Revised: 29 June 2022
Accepted: 11 July 2022

1 Introduction

Due to the long and cold winters in northwest China, the demand for heating is large in this region (BERC 2020). Most of the traditional heating sources are fossil fuels, which results in serious environmental pollution and face resource depletion (Luo et al. 2020; Zhou et al. 2022). To cope with the environment and energy crisis, the energy structure of heating systems in northwest China requires transformation (National Energy Administration of China 2017; Zhou et al. 2021). Solar energy is one of the renewable energies with the largest utilization potential, the most mature technology, and the widest application scope (Chen et al. 2020; Luo et al. 2022b). Northwest China is advantaged by high levels of solar irradiation, which can reach 1,600–2300 kWh/(m^2·a) in Tibet, Qinghai, and Gansu with a total number of 2,800–3,300 annual sunshine hours (Li et al. 2014). Thus, fully utilizing solar energy resources to construct solar heating systems is an effective way to solve the heating issues in northwest China (Luo et al. 2021).

Solar heating systems can be divided into centralized heating systems and distributed heating systems (Miedaner and Pauschinger 2012). In contrast to distributed solar systems, the implementation of centralized systems is most beneficial in areas where users are relatively concentrated. While Sweden is the first country to develop centralized solar heating technology (Huang and Xu 2016), this technology has been developing rapidly in Denmark, Austria, and other European countries. By the end of 2017, 296 large centralized solar heating systems have been constructed in Denmark, with a total installation area of 1,741,344 m^2 (Weiss and Spörk-Dür 2018). The performance of centralized solar heating systems depends highly on the system design. Commonly employed design methods include F diagram

E-mail: xiluo@xauat.edu.cn

(Klein et al. 1976) and φ-F diagram (Klein and Beckman 1979), which both provide the basis for system equipment selection in the form of charts. However, these two methods simplify the centralized solar heating system to a large extent. For example, the F diagram method assumes that the heat loss of solar collectors and the daily average solar radiation intensity are constants, which results in large deviations from the actual operation state of the system. With the development of computer technology, conducting design optimization of solar heating system using simulation methods has become the first choice of many scholars. For example, Long et al. (2020) designed a parallel solar-air heat pump system for office building heating, conducted modeling and simulations in TRNSYS, and optimized key design parameters such as the system equipment capacity. Qiu et al. (2021) proposed a new heating strategy for commercial buildings and used a TRNSYS-based approach to conduct equipment capacity optimization and economic analysis of the system. Also based on TRNSYS, Zhang et al. (2021) conducted a comparative study on auxiliary heat sources suitable for a centralized solar heating system in the Qinghai-Tibet Plateau of China using economy as the evaluation index. The above design methods of centralized solar heating systems based on simulation identify the optimal system design parameters through optimization calculations, which are characterized by high accuracy and reliability.

However, in the mentioned optimization design studies of the centralized solar heating systems, the influence of the heating network on the optimization design of the equipment capacity of the solar heating station was neglected, because the users were all treated as single nodes. Furthermore, in the optimization design of the centralized heating network, scholars often assume that the supply and return water temperature of the heating network is constant, and the heating source and pipe network are decoupled from each other in the centralized heating system. For example, Dobersek and Goricanec (2009) and Wang et al. (2017) established optimization models to optimize the pipe network layout, pipe diameter, and other design parameters of the centralized heating network with economy as the optimization objective. Mertz et al. (2016) simultaneously optimized the design and operating parameters of the centralized heating network with economy as the optimization objective. According to the research results by Pirouti et al. (2013), different operating strategies of the centralized heating system and the temperature setting of supply and return water have a great influence on the pipe diameter design of the heating network. However, as susceptible to weather, the centralized solar heating system requires a more refined system optimization design. Therefore, the research method of decoupling heating source and heating network is not suitable for centralized solar district heating systems, and a joint optimization method has to be applied to the equipment capacity and heating network of a centralized solar district heating system.

At present, in the research on the optimization design of district centralized heating systems using multiple heat sources, in which solar energy is included, a few studies on simultaneous optimization design of system equipment capacity and the heating network were conducted. For example, van der Heijde et al. (2019) proposed a two-layer optimization model of integrated optimization design and control strategy for a district centralized heating system; in the main optimization step, equipment capacity and pipe diameter of the district centralized heating system was optimized by using the genetic algorithm. However, the study only considered the energy balance of the system and not the interconnection of the operating parameters between the heating sources and the heating network. In addition, most of the above studies conduct single-objective optimization, while the optimization design of centralized solar district heating systems requires a comprehensive evaluation of the design scheme based on multiple indicators, such as technology, economy, and environment, and the obtained results cannot provide data or theoretical support for practical engineering projects.

In summary, only a few existing optimization design studies on centralized solar district heating systems consider a simultaneous optimization design for the solar heating station and the centralized heating network, and a large difference exists between the state parameters of the system design and those of the actual operation. Therefore, these design approaches are not suitable to obtain an optimal centralized solar district heating system design. In this study, a joint multi-objective optimization model is established to simultaneously optimize equipment capacity and the pipe diameter of the heating network of the centralized solar district heating system. The main contributions of this paper are as follows:

- A joint multi-objective optimization model for the design of the centralized solar district heating system is established which can optimize equipment capacity and pipe diameter simultaneously.
- To improve the calculation accuracy, detailed hydraulic and thermal calculations are added in the design optimization process of the centralized solar district heating system.
- Comparing the design optimization results of centralized solar district heating systems in typical cities in northwest China, the key influencing factors of the centralized solar district heating system design are analyzed.

The remainder of this paper is arranged as follows. A detailed description and basic numerical models of a centralized solar district heating system are presented in

Section 2. A joint multi-objective optimization model is established in Section 3. This optimization model is applied to case studies, for which the parameters and assumptions are provided in Section 4. Results and discussions of the case studies are presented in Section 5. Finally, the main findings of the present study are summarized in the conclusion section, including some recommendations.

2 System description and basic models

In this study, the centralized solar district heating system is mainly composed of a solar heating station and a centralized heating network. The specific mathematical modeling of the two parts is as follows.

2.1 Solar heating station

The solar heating station is mainly composed of solar thermal collector equipment, heat storage equipment, and auxiliary heat source equipment. Its basic structure (Huang et al. 2019a) is shown in Figure 1.

2.1.1 Solar collector

In this study, the detailed configuration of the solar collector array is not considered in the optimization process, because of the increased difficulty caused by considering the collector configuration in establishing and solving the joint multi-objective optimization model. Instead, the effective area of the solar collector array is selected as the optimization variable (Winterscheid et al. 2017; Huang et al. 2019b; Kubiński and Szabłowski 2020; Zhang et al. 2021). When the effective area of the solar collector array is optimized, the number of certain type of solar collectors can be easily calculated according to the collector specification.

The thermal efficiency of evacuated tube solar collectors is predicted by using Eq. (1) (Dorotić et al. 2019).

$$\eta_{SC,t} = \eta_0 - a_1 \frac{(T_{i,t} - T_{e,t})}{I_t} - a_2 \frac{(T_{i,t} - T_{e,t})^2}{I_t} \quad (1)$$

where $\eta_{SC,t}$ is the thermal efficiency of the solar collector; η_0 is the optical efficiency of the solar collector; a_1 and a_2 are the first-order and second-order efficiency coefficients, respectively; $T_{i,t}$ is the mean solar thermal collector temperature which is often replaced by the inlet water temperature of the solar collector, °C; $T_{e,t}$ is the outdoor air temperature, °C; I_t is the global solar irradiance for ideal azimuth and elevation angles, W/m^2. Solar collector parameters are shown in Table 1.

After acquiring the solar thermal efficiency of the solar collector, the total heat collection of the solar collector can be calculated as follows:

$$Q_{SC,t} = 3.6 A_{SC} \eta_{SC,t} I_t \quad (2)$$

where $Q_{SC,t}$ is the total heat collection of the solar collector per hour, kJ; A_{SC} represents the effective area of the solar collector, m^2.

The solar collector will not be operated if the upper temperature of the water tank is higher than 95 °C. Otherwise, the start or stop of the solar collector pump is controlled by the difference in outlet and inlet temperature: when the outlet water temperature is 8 °C higher than the inlet water temperature, the collector pump will be started; when the temperature difference drops to 4 °C, the collector pump will be stopped.

2.1.2 Heat storage water tank

In this paper, a short-term heat storage water tank is selected

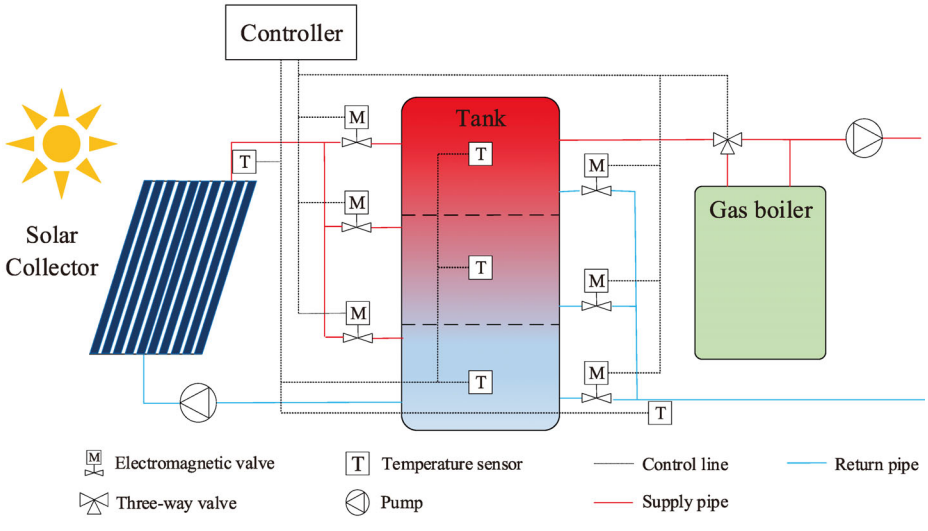

Fig. 1 Solar heating station

Table 1 Solar collector parameters (Carotenuto et al. 2017; Liu et al. 2021)

Parameter	Value	Unit
Optical efficiency η_0	0.80	/
First-order efficiency coefficient a_1	4.68	kJ/(h·m²·K)
Second-order efficiency coefficient a_2	0.03	kJ/(h·m²·K²)
Fluid specific heat c_s	4.19	kJ/(kg·K)
Service time m	15	Years

as the heat storage facility. Since the temperature stratification occurs in the heat storage water tank during operation, the heat storage water tank can be simplified composed of N horizontal mixing zones, where the temperature of zone i is uniform (Wang and Liu 2010), as shown in Figure 2.

The control function F_i of solar collector outlet water entering the water tank is defined as:

$$F_i = \begin{cases} 1 & \text{if } i = 1 \text{ and } T_{co} > T_{s,1} \\ 1 & \text{if } T_{s,i-1} > T_{co} > T_{s,i} \\ 0 & \text{else} \end{cases} \quad (3)$$

where T_{co} is the outlet temperature of the solar collector, °C; $T_{s,i}$ is the water temperature at the i^{th} node of the heat storage water tank, °C.

The control function G_i of return water of the heating network entering the water tank is defined as:

$$G_i = \begin{cases} 1 & \text{if } T_{s,i-1} > T_L > T_{s,i} \\ 1 & \text{if } i = N \text{ and } T_L > T_{s,N} \\ 0 & \text{else} \end{cases} \quad (4)$$

where T_L denotes the return water temperature of the heating network, °C.

The net flow from node i–1 to node i of the heat storage water tank is represented by the mixing flow $Q_{m,i}$. In this paper, only vertical exchange is considered, and the flow directly into the node from the collector or the heating network is not considered.

$$Q_{m,1} = 0 \quad (5)$$

$$Q_{m,i} = Q_c \sum_{j=1}^{i-1} F_j - Q_L \sum_{j=1}^{N} G_j \quad (6)$$

$$Q_{m,N+1} = 0 \quad (7)$$

where Q_c and Q_L denote the circulating volume flow on the solar collector side and the heating network side, respectively, m³/h.

Based on the above control functions and mixing flows, the energy balance equation of node i can be obtained.

$$V_{s,i}\frac{dT_{s,i}}{d\tau} = F_i Q_c (T_{co} - T_{s,i}) - G_i Q_L (T_{s,i} - T_L) - \frac{U_s E_{s,i}}{\rho c_s}(T_{s,i} - T_e) + \begin{cases} Q_{m,i}(T_{s,i-1} - T_{s,i}), \text{if } Q_{m,i} > 0 \\ Q_{m,i+1}(T_{s,i} - T_{s,i+1}), \text{if } Q_{m,i+1} < 0 \end{cases} \quad (8)$$

where $V_{s,i}$ is the volume of node i in the water tank, m³; U_s is the heat loss coefficient of the water tank, which is equal to 0.4 W/(m²·°C); $E_{s,i}$ is the surface area of water tank node i, m²; c_s is the specific heat capacity of water, kJ/(kg·K); ρ is the density of water, kg/m³.

This paper adopts a three-node water tank stratification model.

2.1.3 *Auxiliary heat source*

A natural gas hot water boiler with a quick response time is adopted as the auxiliary heat source in the centralized solar district heating system, and the heat produced per time unit can be calculated by using Eq. (9).

$$Q_{GB} = 3600\eta_{gb,x}\eta_{gb}P_{GB} \quad (9)$$

where Q_{GB} is the heat provided by the gas boiler per hour, kJ; the value 3600 is the conversion coefficient between the units

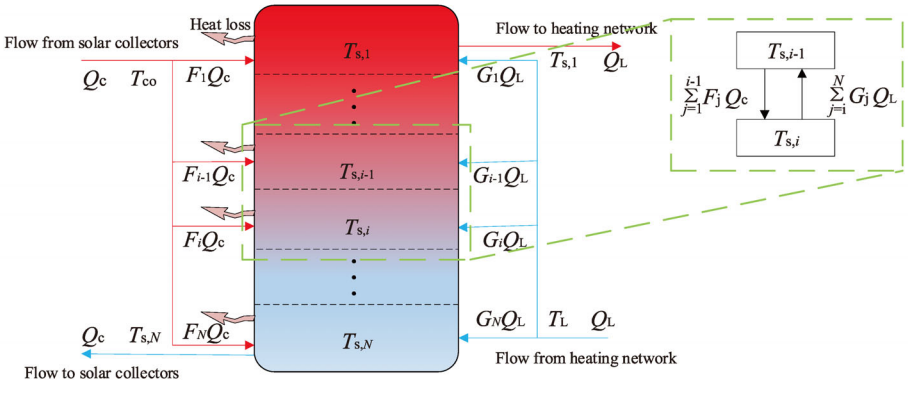

Fig. 2 Schematic of the heat storage water tank stratified into N nodes. T denotes temperature, Q denotes the circulating flow, F_i and G_i are control functions

of time, i.e., 1 hour is 3600 seconds; $\eta_{gb,x}$ is the operation load rate of the gas boiler, which depends on the heat requirements of the system; η_{gb} is the operation efficiency of the gas boiler, which is equal to 0.85; P_{GB} is the rated power of the gas boiler, kW.

The start and stop of the auxiliary heat source are controlled by temperature: when the upper temperature of the water tank is below the minimum water supply temperature, the auxiliary heat source is started; when the temperature is higher than the minimum water supply temperature, the auxiliary heat source is stopped.

Technical Handbook for Solar Heat Supply and Space Heating (He and Zhu 2009), the relevant design code in China, mentions that the centralized solar heating system operates at a low temperature compared with the centralized heating system using conventional energy to ensure the highly efficient operation of the solar collectors. When using the radiant floor heating to heat users of the centralized heating system, *JGJ142-2004 Technical Specification for Floor Radiant Heating* (MOHURD 2004), the relevant design code in China, requires that the hot water temperature through the user should not be lower than 30 °C. Besides the large heat loss of the centralized heating network, the minimum water supply temperature is equal to 50 °C in this study.

2.2 Centralized heating network

Commonly, the centralized heating network has three typical grid topologies, which are the radial grid, the ring grid, and the meshed grid. The radial grid represents the tree topology, in which root represents the heat source and branches represent the heating pipes of the centralized heating system (von Rhein et al. 2019). Since the investment cost of the radial grid is the lowest, this paper selects the radial grid network as an example for analysis.

2.2.1 Hydraulic model of the heating network

Pressure loss of heating networks includes major head loss and local pressure loss as shown in Eq. (10).

$$\Delta P_{total} = \Delta P_{pipe} + \Delta P_{local} \tag{10}$$

where ΔP_{total} is the total pressure loss of heating networks, Pa; ΔP_{pipe} is the major head loss, Pa; ΔP_{local} is the local pressure loss, Pa.

The major head loss is calculated by Eqs. (11)–(13) (Wang et al. 2017; Wang et al. 2018).

$$\Delta P_{pipe} = \sum R_k \tag{11}$$

$$R_k = f_k \frac{8\rho L_k (Q_k / 3600)^2}{\pi^2 (d_k)^5} \tag{12}$$

$$f_k = 0.11\left(\frac{K}{d_k} + \frac{68}{Re}\right)^{0.25} \tag{13}$$

where R_k denotes the hydraulic head loss caused by friction in pipe section k, Pa; f_k is the friction coefficient of pipe section k; Q_k is the flow rate in pipe section k, m^3/h; L_k and d_k denote the pipe length and diameter in pipe section k, respectively, m; K is the equivalent roughness height of the heating pipe, which is equal to 0.005; Re is the Reynolds number of the fluid in the heating pipe.

The local pressure loss is usually estimated based on the calculated major head loss as shown in Eq. (14).

$$\Delta P_{local} = \delta \Delta P_{pipe} \tag{14}$$

where δ is equal to 0.25.

Table 2 lists the dimensions parameters of the district heating network.

2.2.2 Thermal model of the heating network

The relevant water temperatures at each node of the heating network are calculated as follows (Ayele et al. 2018):

$$T_{out} = (T_{in} - T_e)e^{-\lambda_k L_k/(c_s \rho Q_k)} + T_e \tag{15}$$

$$\left(\sum Q_{mix,out}\right) T_{mix,out} = \sum (Q_{mix,in} T_{mix,in}) \tag{16}$$

Table 2 Parameters of the district heating network

Nominal diameter of the pipe (*DN*) (mm)	Thickness of steel pipe (mm)	Thickness of polyurethane insulation material (mm)	Thickness of high-density polyethylene sheath (mm)
100	4	15	3
150	4.5	20	
200	6	20	
250	6	25	
300	7	25	
350	7	35	
400	7	35	
450	7	40	

where T_{in} and T_{out} denote the inlet and outlet temperature of a pipe section, respectivley, °C; λ_k is the heat transfer coefficient of pipe section k, W/(m·K); $Q_{mix,out}$ and $T_{mix,out}$ are the water flow rate (m³/h) and the water temperature (°C), respectivley after hot water confluence from a multi-pipe section; $Q_{mix,in}$ and $T_{mix,in}$ denote the water flow rate (m³/h) and the water temperature (°C), respectively in the pipe section before confluence.

Table 3 lists the heat transfer parameters of the district heating network.

The heat exchange equations of the secondary heat exchange station at the user place are as follows:

$$\Phi_n = \varepsilon \rho c_s Q_n \left(T_{supply,n} - T_n \right) \tag{17}$$

$$\Phi_n = \rho c_s Q_n \left(T_{supply,n} - T_{return,n} \right) \tag{18}$$

where Φ_n is the heating load of user n, kJ; ε is the heat exchange efficiency of the secondary heat exchange station, which is equal to 0.80; Q_n is the water supply flow of the primary network of the secondary heat exchange station at the place of user n, m³/h; $T_{supply,n}$ and $T_{return,n}$ respectivley denote the inlet and outlet water temperature of the primary network of the secondary heat exchange station at the place of user n, °C; T_n is the inlet water temperature of the secondary network of the secondary heat exchange station at the place of user n, °C;

According to Eq. (15), with increasing water supply flow in the same pipe section, the drop of hot water temperature in the pipe decreases, and the water temperature at the user place increases. According to Eq. (17), with increasing water temperature at the user place, the water supply flow required by the user decreases. The water supply flow required by the user and the heating water temperature at the user place influence each other; thus, this paper adopts the method of stepwise correction to determine the water supply flow Q_k of the heating network, the flow chart of which is shown in Figure 3.The specific steps are as follows.

Step 1: Ignore the heat loss of the pipe network. Assume the water supply temperature of the water tank as the inlet temperature of the primary network of the secondary heat exchange station at the user place, then calculate the water supply flow required by the user by using Eq. (17) combined with the user heating load, and finally calculate the water supply flow of all pipe sections of the heating network.

Table 3 Heat transfer parameters of the district heating network

Component	Coefficient of heat transfer ($W \cdot m^{-2} \cdot °C^{-1}$)
Steel	45
Polyurethane insulation material	0.023
High-density polyethylene sheath	0.3

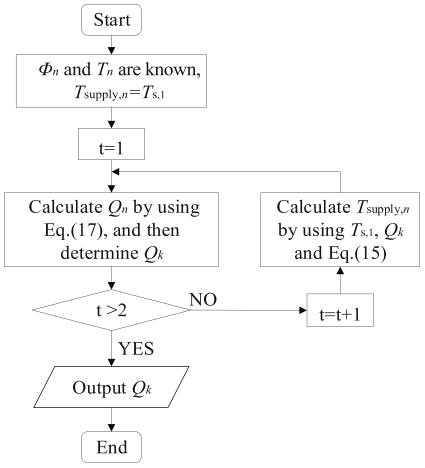

Fig. 3 The flow chart of calculating the water supply flow of each section of the centralized heating network, in which t represents the step of the calculation

Step 2: In combination with the water supply temperature of the water tank and the water supply flow of each pipe section obtained from the previous step, Eq. (15) is used to calculate the inlet temperature of the primary network of the secondary heat exchange station at the user place, and then the new water supply flow of all pipe sections of the heating network are obtained.

Step 3: Repeat the previous step. The water supply flow in the heating network is modified again.

In the radial grid heating network, the supply and return water flow of each pipe section is the same. Using the above method, the supply and return water flow of each pipe section and the inlet temperature of the primary network of the secondary heat exchange station at the user place can be obtained. Combined with Eq. (18), the outlet temperature of the primary network of the secondary heat exchange station can be determined. Finally, the return water temperature of the heating network entering the water tank can be calculated.

When the user heating load is small, the water supply flow is also small and results in a high decrease in hot water temperature of the heating network so that the inlet temperature of the primary network of the secondary heat exchange station at the user place is too low to provide the temperature difference required for heat exchange. Therefore, a minimum water supply flow is set in the model to meet the temperature difference required for heat exchange at the user place. In this study, the minimum water supply flow is equal to 7 m³/h, which can ensure that the reduced temperature of water through 10,000 meters heating network is not more than 15 °C, while the water supply temperature is 50 °C.

3 Optimization model

3.1 Objective functions

The traditional district centralized heating system using fossil energy releases a large amount of carbon dioxide by burning fossil fuels during the operation of the system, while the use of district centralized solar heating can effectively reduce the emission of carbon dioxide. However, the initial investment cost of solar energy equipment is high at the present stage. Therefore, there is a negative correlation between environmental protection and the economy of the centralized solar heating system. In this paper, a joint multi-objective optimization model for equipment capacity and pipe diameters of a centralized solar district heating system is established with the optimization objective to minimize life cycle cost and CO_2 emissions of this heating system.

3.1.1 *Life cycle cost*

The life cycle cost of the centralized solar district heating system can be calculated as follows:

$$C = C_o + C_r m \frac{i(1+i)^m}{(1+i)^m - 1} - C_{oc} \tag{19}$$

where C_o denotes the operating cost of the system during its useful life, Yuan; C_r is the initial investment cost of the system, Yuan; i is the discount rate, which is equal to 8% (Liu et al. 2021); m is the service life of the system, which is equal to 15 years; C_{oc} is the net residual value of fixed assets (generally 3%–5% of their original value (Wang 2017)), Yuan.

1) Initial investment cost of the system

The initial investment cost of the centralized solar district heating system includes two parts: the cost of the system heating station and the cost of the heating network. The calculation equation is as follows:

$$C_r = A_{SC} C_r^{SC} + P_{GB} C_r^{GB} + V_S C_r^S + C_r^{pump}(P_{p,c} + P_{p,L}) + C_r^{pipe} L \tag{20}$$

where C_r^{SC} is the initial investment cost of the solar collector per unit area (including construction and installation), Yuan/m^2; C_r^{GB} is the initial investment cost of the gas boiler set per rated power unit (including construction and installation), Yuan/kW; C_r^S is the initial investment cost of the heat storage water tank per volume unit (including construction and installation), Yuan/m^3; C_r^{pump} denotes the initial investment cost of the water circulation pump per rated power unit, Yuan/kW; $P_{p,c}$ and $P_{p,L}$ are the rated power values of the water circulation pumps of the solar collector and the centralized heating network, respectively, kW; C_r^{pipe} is the initial investment cost of the heating network per unit length related to the pipe diameter (including construction and installation), Yuan/m; L denotes the pipe length, m.

2) Operating cost of the system during its useful life

The operating cost of the centralized solar district heating system includes the operating costs of the gas boiler, the water circulation pump, the water supplement, and equipment maintenance and is calculated as follows:

$$C_o = \sum_{i=1}^{m} (C_o^{GB} + C_o^{pump} + C_o^{water}) + C_f \tag{21}$$

where C_o^{GB} is the annual operating cost of the gas boiler, Yuan; C_o^{pump} is the annual operating cost of the water circulation pumps; C_o^{water} denotes the annual water supplement cost, Yuan; C_f is the equipment maintenance cost (2% of the total initial investment cost of the system (KO 2015)), Yuan.

$$C_o^{GB} = V_{Gas} C_{gas} \tag{22}$$

$$V_{Gas} = \frac{\sum_{t=1}^{M} Q_{GB}}{H_i \eta_{gb}} \tag{23}$$

where V_{Gas} is the annual volume of natural gas consumed, m^3; C_{gas} is the price of natural gas, Yuan/m^3; H_i is the calorific value of natural gas, 39×10^3 kJ/m^3; M denotes the annual heating hours in a heating period.

$$C_o^{pump} = W_{Ele} D_s \tag{24}$$

$$W_{Ele} = \sum_{t=1}^{M} \left(\frac{\rho g H_c Q_c}{3600000 \eta_c} + \frac{\rho g H_L Q_L}{3600000 \eta_L} \right) \tag{25}$$

where W_{Ele} is the annual electricity consumption of the water circulation pumps, kWh; D_s is the local electricity price, Yuan/kWh; g is the acceleration of gravity, m/s^2; H_c and H_L are the pump heads of the solar collector pump and the centralized heating network pump, respectively, m; η_c and η_L are the efficiencies of the water circulation pumps of solar collector and the centralized heating network, respectively, which is equal to 0.75.

$$C_o^{water} = \sum_{t=1}^{M} (Q_c \eta_{bs,c} + Q_L \eta_{bs,L}) J_s \tag{26}$$

where $\eta_{bs,c}$ and $\eta_{bs,L}$ denote the water supplement rate at the solar collector side and the centralized heating side of the system, respectively, which is equal to 0.02; J_s is the water price, Yuan/m^3.

Table 4 lists the economic calculation parameters of the centralized solar district heating system.

Table 4 Economic inputs for system optimization (Huang et al. 2019b; Liu et al. 2021; State Grid of China 2022)

Item		Value	Unit
Collector C_r^{SC}		1000	¥/m²
Gas boiler C_r^{GB}		500	¥/kW
Heat storage water tank C_r^{S}		500	¥/m³
Pump C_r^{pump}		1000	¥/kW
Electricity D_s	Lhasa	0.69	¥/kWh
	Xining	0.43	
	Xi'an	0.65	
Gas C_{gas}		3	¥/m³
Water J_s		3	¥/t
District heating network	Steel	4,500	¥/t
	Polyurethane insulation material	42,000	
	High-density polyethylene sheath	11,500	

Note: The initial cost of the solar collector and relevant pipes is converted into the cost per effective area of the solar collector (Kubiński and Szabłowski 2020; Zhang et al. 2021), which is presented in the table.

3.1.2 *Life cycle carbon dioxide emission*

The CO_2 emission of the centralized solar district heating system during its life cycle mainly includes carbon dioxide produced during equipment production and system operation.

$$M_{CO_2} = M_{CO_2,e} + M_{CO_2,o} \tag{27}$$

where M_{CO_2} is the life cycle CO_2 emission of the system; $M_{CO_2,e}$ is the CO_2 emission during equipment production, t; $M_{CO_2,o}$ denotes the CO_2 emission during system operation, t.

1) Carbon dioxide emission during equipment production

The equation to calculate the CO_2 emission generated by each piece of equipment in the production stage of the centralized solar district heating system is as follows:

$$M_{CO_2,e} = m_{CO_2}^{SC} A_{SC} + m_{CO_2}^{GB} P_{GB} + m_{CO_2}^{S} E_S + m_{CO_2,pump}(P_{p,c} + P_{p,L}) + m_{CO_2,pipe} \tag{28}$$

where $m_{CO_2}^{SC}$ is the CO_2 emission from the production of the solar collector per unit area, $kgCO_2/m^2$; $m_{CO_2}^{GB}$ is the CO_2 emission from the production of the gas boiler set per unit rated power, $kgCO_2/kW$; $m_{CO_2}^{S}$ is the CO_2 emission from the production of the water tank per unit surface area, $kgCO_2/m^2$; E_S is the surface area of the water tank, m^2; $m_{CO_2,pump}$ is the CO_2 emission of the production of a water circulation pump per unit rated power, $kgCO_2/kW$; $m_{CO_2,pipe}$ denotes the CO_2 emissions from the production of the centralized heating network, $kgCO_2$.

2) Carbon dioxide emission during system operation

The CO_2 emission from the operation of the centralized solar district heating system mainly includes the CO_2 emission from the operation of the gas boiler and the water circulation pumps and is calculated as follows:

$$M_{CO_2,o} = \sum_{i=1}^{m}\left(m_{CO_2}^{Gas}\rho_{Gas}V_{Gas} + m_{CO_2}^{Ele}W_{Ele}\right) \tag{29}$$

where $m_{CO_2}^{Gas}$ is the CO_2 emission caused by burning natural gas per unit mass, $kgCO_2/kg$; ρ_{Gas} is the density of natural gas, kg/m^3; $m_{CO_2}^{Ele}$ is the CO_2 emission caused by the operation of the pumps of per unit electricity, $kgCO_2/kWh$.

Table 5 lists the carbon dioxide emission calculation parameters of the centralized solar district heating system.

3.2 Decision variables

Decision variables in this study are the equipment capacity parameters A_{SC}, V_S, and P_{GB}, as well as the pipe diameter of the centralized heating network.

3.3 Constraints

1) Solar fraction

The solar fraction of the centralized solar district heating system is calculated as follows:

$$FR = \frac{Q_{SC}}{Q_{system}} \tag{30}$$

where FR is the solar fraction; Q_{SC} is the total heat of the solar collector, kJ; Q_{system} is the total heating load demand of the system, kJ.

In *GB 50495-2019 Technical Standard for Solar Heating System* (MOHURD 2019), the relevant design code in China, the recommended range of solar fraction is listed for regions with different levels of solar energy resource

Table 5 Carbon dioxide emission inputs for system optimization (Ding et al. 2020; Shah et al. 2020)

Item		Value	Unit
Collector $m_{CO_2}^{SC}$		131.74	$kgCO_2/m^2$
Gas boiler $m_{CO_2}^{GB}$		50	$kgCO_2/kW$
Heat storage water tank $m_{CO_2}^{S}$		243	$kgCO_2/m^2$
Pump $m_{CO_2,pump}$		30	$kgCO_2/kW$
Electricity $m_{CO_2}^{Ele}$		0.70	$kgCO_2/kWh$
Gas $m_{CO_2}^{Gas}$		2.98	$kgCO_2/kg$
District heating network	Steel	3.15	t/t
	Polyurethane insulation material	5.22	
	High-density polyethylene sheath	2.62	

abundance, as shown in Table 6. In the joint multi-objective optimization model of a centralized solar district heating system in this paper, the system solar fraction is only constrained to be greater than the minimum recommended value.

2) Water supply velocity and specific friction resistance of the centralized heating network

CJJ 34-2010 Design Code for City Heating Network (MOHURD 2010), the relevant design code in China, requires that the flow rate in the heating network with $DN \geq 400$ mm (nominal diameter of pipe ≥ 400 mm) should not exceed 3.5 m/s, and the specific friction resistance of a heating network with $DN < 400$ mm should not exceed 300 Pa/m. Thus,

when $DN \geq 400$ mm,

$$\frac{4Q_k}{3600\pi d_k^2} \leq 3.5 \text{ m/s} \tag{31}$$

when $DN < 400$ mm,

$$\frac{R_k}{L_k} \leq 300 \text{ Pa/m} \tag{32}$$

3.4 Solving method

In contrast to single-objective optimization, a set of optimal solutions can be obtained via multi-objective optimization, each of which is called a Pareto-optimal solution or non-inferior optimal solution. Genetic algorithm is widely used in district system optimization, and elitist non-dominated sorting genetic algorithm (NSGA-II) is commonly used in multi-objective optimization (Evins 2013). Therefore, the NSGA-II algorithm is used in this study, the flow chart of which is shown in Figure 4. Selecting one hour as the time step and the entire heating season as the calculation cycle, the optimization model is solved in MATLAB.

In this study, the population size and maximum iteration number are set respectively to 80 and 200, to obtain sufficiently accurate results at a reasonable calculation time.

Table 6 Recommended range of solar fraction for a centralized solar district heating system in different areas of China

Solar energy resource zoning	Recommended value range of solar fraction	Typical city
Rich resource area	≥50%	Lhasa, Golmud
Abundant resource area	30%–50%	Xining, Turpan and Kashgar
Relatively rich resource area	20%–40%	Xi'an, Lanzhou, Urumqi
General resource area	10%–30%	Chengdu, Changsha, Wuhan

The crossover operators are widely used to promote the optimization to converge, while the mutation operators are mainly used to maintain the diversity of the genetic population. The probability of mutation should generally remain very low to avoid unnecessarily delay in optimization (Ren et al. 2019). And the variable search ranges are shown in Table 7.

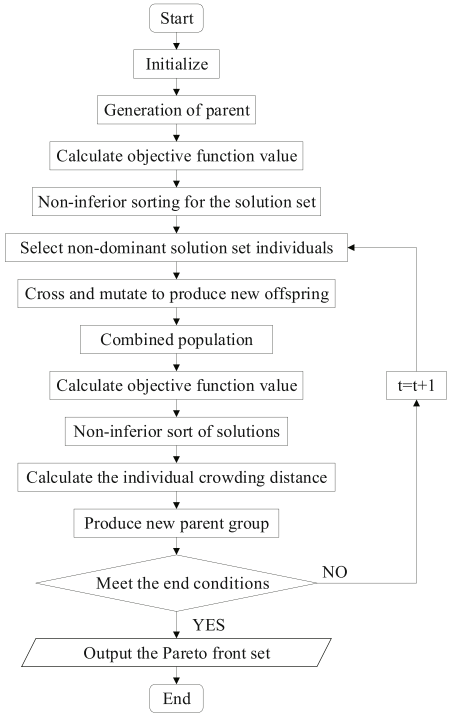

Fig. 4 The flow chart of NSGA-II, in which *t* represents iterations (Wang et al. 2019)

Table 7 The upper and lower limits of the optimization variables

City	Optimization variable	Upper limit	Lower limit
Lhasa	The area of solar collector (m^2)	25,000	2,000
	The volume of water tank (m^3)	4,000	300
	The rated power of the gas boiler (kW)	8,000	800
	The diameter of heating network pipe (mm)	400	100
Xining	The area of solar collector (m^2)	65,000	5,000
	The volume of water tank (m^3)	15,000	500
	The rated power of the gas boiler(kW)	20,000	2,000
	The diameter of heating network pipe (mm)	450	100
Xi'an	The area of solar collector (m^2)	65,000	5,000
	The volume of water tank (m^3)	20,000	500
	The rated power of the gas boiler(kW)	20,000	3,000
	The diameter of heating network pipe (mm)	450	100

Note: The optimization variables of the heating network pipe diameters can only be selected from the following values: 100, 150, 200, 250, 300, 350, 400 and 450 mm.

Technique for Order Preference by Similarity to an Ideal Solution (TOPSIS) is a popular and efficient technique used for identifying the best design in multi-objective optimization problems. First, the method determines the non-ideal solution and ideal solution by considering the best and the worst designs of every attribute. Then, the values of every attribute are set as non-dimensional. Finally, the TOPSIS rank index is calculated by Eq. (33), which is used to rank the Pareto frontier in decreasing order.

$$D_{\text{topsis}} = \frac{d^-}{d^- + d^+} \tag{33}$$

where d^- is the distance from the alternative to the non-ideal solution, and d^+ is the distance from the alternative to the ideal solution.

4 Case study

The joint multi-objective optimization model formulated in Section 3 is applied to case studies.

4.1 Centralized solar district heating system

The centralized solar district heating system and the building distribution in the calculation example of this study are shown in Figure 5. Users 1 and 4 are residential buildings with heating areas of 74,800 m^2 and 46,800 m^2, respectively. User 2 is a commercial building and User 3 is an office building with heating areas of 51,800 m^2 and 58,100 m^2, respectively.

4.2 Heating load of different buildings

Geometries of residential, commercial, and office buildings are constructed in SketchUp, as shown in Figure 5. EnergyPlus is then used to conduct hourly simulations of the building heating load in winter (Luo et al. 2022a). The main simulation parameters of the various buildings are shown in Table 8.

For the winter heating period, the hourly heating load simulation results of each user in the three cities are shown in Figure 6.

In Figure 6, Xining has the coldest weather and longest heating period, and the annual total heating load of local users is the largest. The Xi'an area has the least solar energy resources and therefore a large annual total heating load, while Lhasa has the most abundant solar energy resources and the lowest annual total heating load of users. In addition, as the solar energy resources in Lhasa are the most abundant,

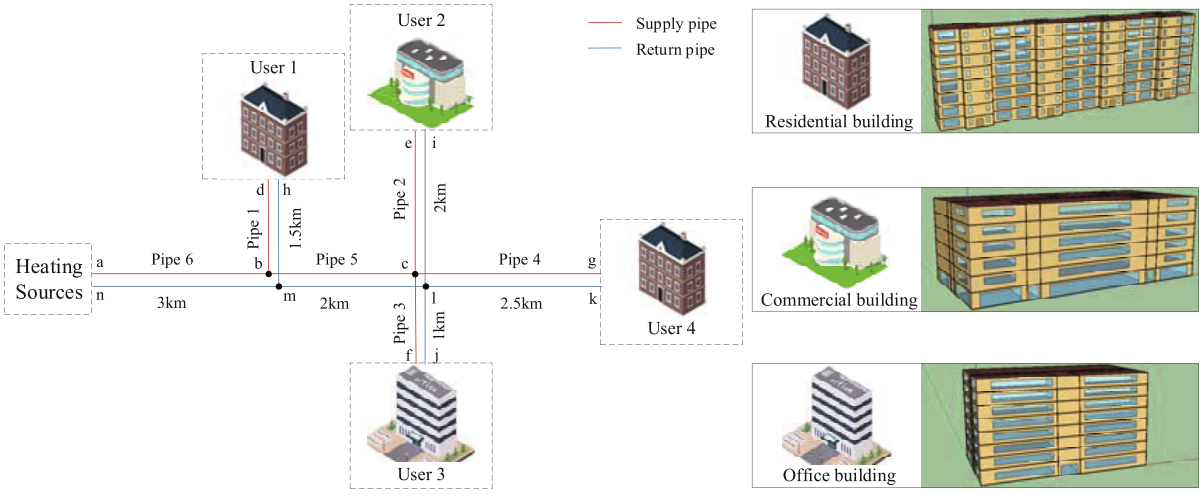

Fig. 5 Distribution of the centralized solar district heating system and buildings

Table 8 Building heating load simulation parameters

City	Heat transfer coefficient of residential building envelope structures (W·m^{-2}·K^{-1})			Heat transfer coefficient of commercial and office building envelope structures (W·m^{-2}·K^{-1})			Heating period
	Wall	Roof	Window	Wall	Roof	Window	
Lhasa	0.407	0.211	1.800	0.407	0.365	1.800	11/15–3/15
Xining	0.358	0.174	1.800	0.358	0.246	1.800	10/15–4/15
Xi'an	0.407	0.246	1.800	0.407	0.365	1.800	11/15–3/15

Note: The parameter values in the table are in line with the relevant design code in China (MOHURD 2015, 2018).

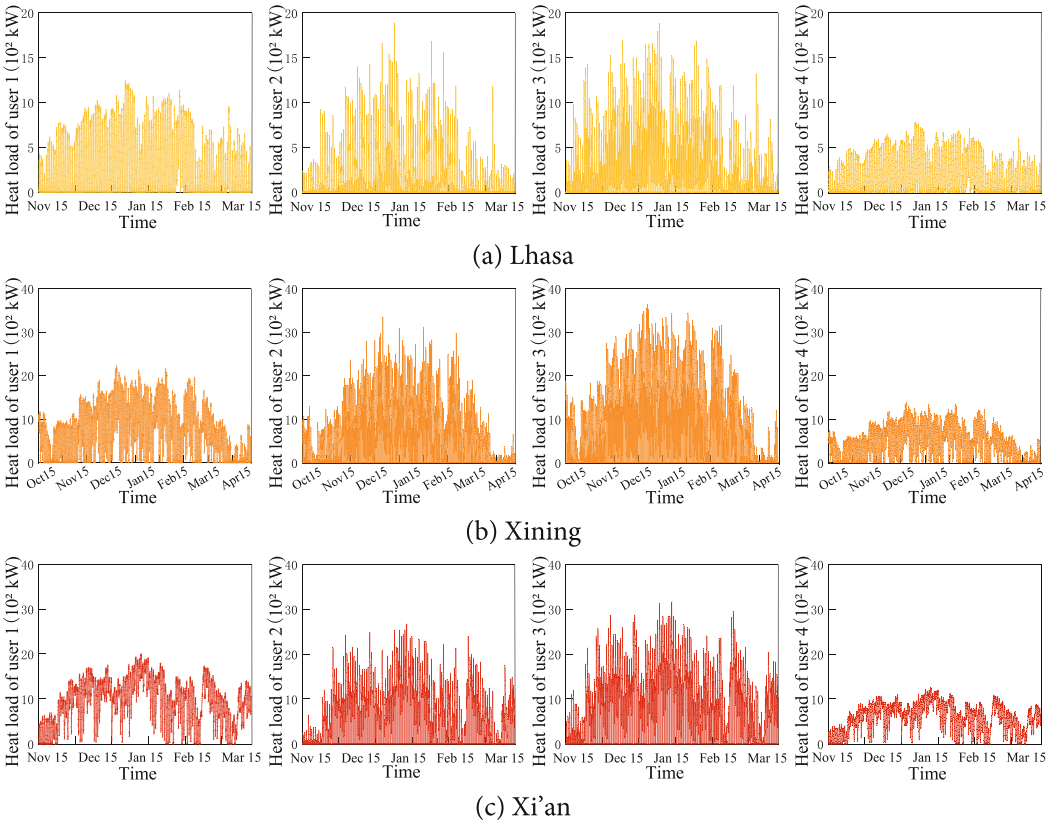

Fig. 6 Hourly heating load of residential, commercial, and office buildings in three cities during the heating period

the heating load in winter is small in the daytime and even zero in the afternoon. Compared with Xining and Xi'an, Lhasa has the largest proportion of time with a low heating load in the heating period.

5 Results and discussion

5.1 Analysis of the joint multi-objective design optimization results of the system

Using Lhasa, Xining, and Xi'an as examples, joint multi-objective design optimization of the centralized solar district heating system was carried out in the heating areas in this study. The Pareto frontier of the optimized design results is shown in Figure 7.

In Figure 7, A and C denote the design schemes of the centralized solar heating system with optimal economy and optimal environmental protection, respectively, while B represents the comprehensive optimal solution obtained with the TOPSIS decision method. The specific design parameters of the three schemes in each city are shown in Figure 8.

In Figure 8, the obtained optimized design schemes of centralized solar district heating systems in the three cities reveal that with the decrease in system economy and the increase in environmental protection, the pipe diameter of

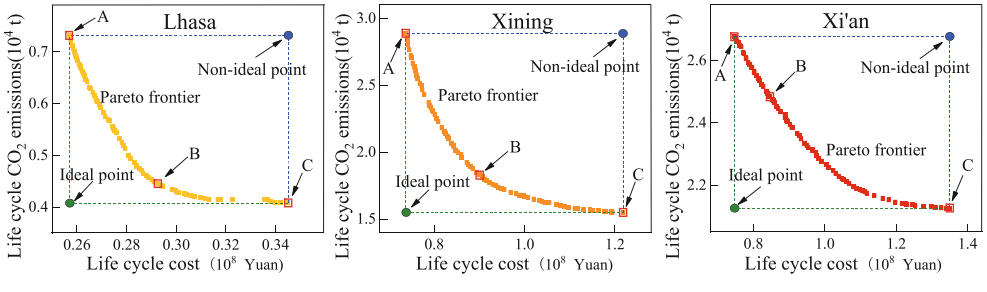

Fig. 7 Pareto frontier of joint multi-objective design optimization of centralized solar district heating systems in Lhasa, Xining, and Xi'an. A, B and C denote the economic optimal, the comprehensive optimal and the environmental optimal design schemes of system, respectively

		A_{SC} (m^2)	V_S(m^3)	P_{GB} (kW)	Pipe Diameter (mm) 150 200 250 350						FR
					Pipe 1	Pipe 2	Pipe 3	Pipe 4	Pipe 5	Pipe 6	
Lhasa	Economic-optimal	4,366	866	5,883	150	200	200	150	250	250	0.50
	Comprehensive-optimal	10,629	1,795	3,240	150	200	200	150	250	250	0.90
	Environmental-optimal	14,981	2,059	1,761	150	150	200	150	250	250	0.99
Xining	Economic-optimal	10,543	1,087	11,664	200	200	200	150	350	350	0.30
	Comprehensive-optimal	30,383	5,163	9,678	200	200	200	200	350	350	0.70
	Environmental-optimal	54,496	8,903	6,263	200	200	200	250	350	350	0.93
Xi'an	Economic-optimal	14,139	1,278	9,538	200	200	200	200	300	350	0.20
	Comprehensive-optimal	21,778	2,842	9,465	200	200	200	200	350	350	0.31
	Environmental-optimal	53,837	12,233	8,723	200	200	200	250	350	350	0.66

Fig. 8 Results of joint multi-objective design optimization of centralized solar district heating systems in Lhasa, Xining, and Xi'an

the centralized heating network in Lhasa tends to decrease while that in Xining and Xi'an tends to increase. As an explanation, the annual total heating load of users is the smallest in Lhasa, and the time of users requiring a low heating load in the heating period accounts for the largest proportion, which results in the lowest CO_2 emission from the operation of the water circulation pumps of the system, which is less than the CO_2 emission caused by the construction of the heating network. Therefore, to improve the environmental protection by the system, the diameter of the pipe network should be decreased to reduce the CO_2 emission from the construction of the heating network. For the systems in Xining and Xi'an, the CO_2 emission from the operation of the water circulation pumps is always greater than that caused by the construction of the heating network. Therefore, the network pipe diameter needs to be increased to reduce the CO_2 emission from the operation of the water circulation pumps and improve the environmental protection by the system.

With the decrease in system economy and the increase in environmental protection, the solar fraction increases because of the increase in solar equipment capacity. The design value of the solar fraction in the Lhasa area should be between 50% and 99%, and the optimal value is 90%. In Xining, the solar fraction is between 30% and 93% with an optimal value of 70%. In Xi'an, the solar fraction lies between 20% and 66%, and the optimal value is 31%. Since the Lhasa area has the most abundant solar energy resources among the three cities, it also features the largest solar fraction of the optimal comprehensively designed heating system.

5.2 Analysis of operation results of the systems designed by joint multi-objective optimization

According to the meteorological data of each city, the day closest to the average temperature of the coldest month was selected as the typical design day. The typical days for Lhasa, Xining, and Xi'an are January 17, January 3, and January 19, respectively. Taking a typical heating design day in winter as an example, the system operation of the comprehensive optimal design of the centralized solar district heating system is analyzed. The results are shown in Figure 9.

In Figure 9, on a typical design day in winter, the heat storage water tank temperature of the centralized solar district heating system in Lhasa is relatively higher, and the natural gas boiler does not need to provide auxiliary heating. Since the temperature of the heat storage water tank in Xining and Xi'an is lower, the natural gas boiler has to be used to ensure that the water supply temperature of the system is not lower than the design value of the minimum water supply temperature of the system. In addition, as the user heating load in Lhasa is small or even zero between 15:00 and 18:00, the minimum water supply flow is set for most pipe sections to avoid that the water supply flow is too small to meet the temperature difference required for heat exchange of the secondary heat exchange station at the user place and the return temperature of the heating network has a large fluctuation, which causes great disturbance to the lower layer temperature of the heat storage water tank.

5.3 Comparative analysis of design optimization results with different methods

A comparative method for the design optimization of a centralized solar district heating system is used to verify the superiority of the method proposed in this study. Method 1 is the method proposed in this paper, which is to simultaneously optimize the design of the solar heating station and the centralized heating network. Method 2 is the control method, which is to optimize the design of the solar heating station and the centralized heating network.

In method 2, system operating parameters are assumed according to the average values in the coldest month of the system obtained in method 1, that is, the heat loss of the pipe network per unit length in Lhasa, Xining, and Xi'an is set to be 18 W/m, 21 W/m, and 19 W/m, respectively, and the supply and return water temperatures of the centralized heating network are 50 °C and 30 °C, respectively. The system design results of the two optimization methods are shown in Table 9.

In Table 9, compared with method 2, the equipment capacities and pipe network diameters of the centralized

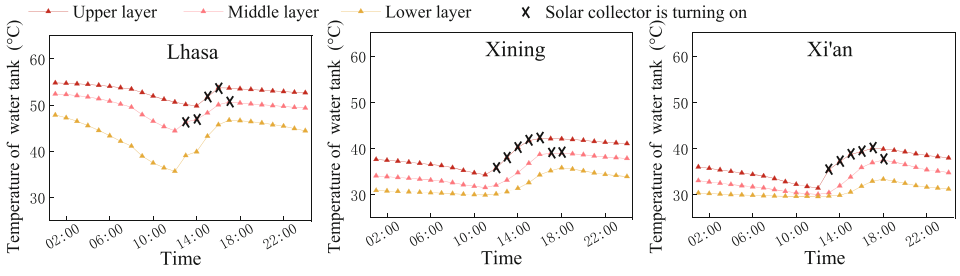

(a) The temperature of the working fluid in the water tank

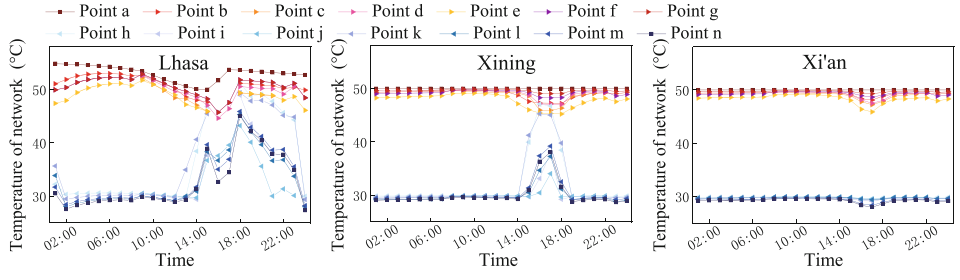

(b) The temperature of the working fluid in the network

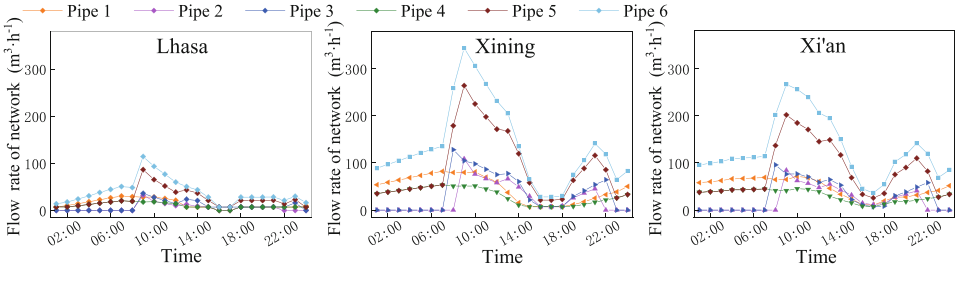

(c) The flow rate of the working fluid in the network

Fig. 9 Operation of the comprehensive optimal design of the centralized solar district heating system on a typical design day in winter

Table 9 Design results of two optimization design methods for centralized solar district heating systems

City		Lhasa		Xining		Xi'an	
Method		1	2	1	2	1	2
Area of the solar collector (m^2)		10,629	12,559	30,383	33,879	21,778	21,157
Volume of the water tank (m^3)		1,795	2,020	5,163	4,112	2,842	2,010
Rated power of the gas boiler (kW)		3,240	3,356	9,678	10,109	9,465	9,695
Diameter of district heating network pipes(mm)	Pipes 1, 2	150, 200	150, 200	200, 200	200, 200	200, 200	200, 200
	Pipes 3, 4	200, 150	200, 150	200, 200	200, 200	200, 200	200, 200
	Pipes 5, 6	250, 250	250, 250	350, 350	350, 350	350, 350	300, 350
Life cycle cost (10^6 ¥)		29.26	33.35	89.36	96.70	84.64	87.45
Life cycle CO_2 emission (10^3 t)		4.45	5.08	18.47	20.78	24.83	27.92

solar district heating system designed by method 1 are more reasonable, the economic costs of the systems are lower, and the environmental performances of the cases are better in the three cities. The life cycle costs of the systems in Lhasa, Xining, and Xi'an are reduced by 12.26%, 7.59%, and 3.21%, respectively, and the life cycle CO_2 emissions of the systems have decreased by 12.40%, 11.12%, and 11.07%, respectively.

5.4 Sensitivity analysis of joint multi-objective system optimization results

In the joint multi-objective optimization of the centralized solar district heating systems, the value of the input parameters exhibits a great influence on the system optimization results. The value of the minimum water supply temperature of the system directly affects the required system equipment capacity and the diameter of the heating network pipes. Equipment price fluctuations also directly affect the economy of the system. Therefore, the sensitivity analysis of joint multi-objective system optimization results is conducted for the variables minimum water supply temperature and equipment unit price.

5.4.1 Minimum water supply temperature

Using the joint multi-objective optimization model developed in this study, the centralized solar district heating system is simulated for different minimum water supply temperatures to analyze its effect on the results of system optimization. Since the heating supply temperature of the fourth generation centralized heating system (low-temperature heating system) is between 30 and 70 °C (Lund et al. 2014) and to ensure stable heating of the system, the simulated minimum water supply temperatures are 45 °C, 50 °C, 55 °C, 60 °C, and 65 °C, respectively. The results are shown in Figure 10.

In Figure 10, with the increase in the minimum water supply temperature, the life cycle cost and CO_2 emission of the centralized solar district heating system in Lhasa both first decrease and then increase, and the optimal minimum water supply temperature is 55 °C. The life cycle cost of the system in Xining decreases first and then increases, while the life cycle CO_2 emissions increase over the selected minimum water supply temperature range. For optimal economy or optimal environmental protection, the minimum water supply temperatures are 50 °C and 45 °C, respectively. With increasing minimum water supply temperature in the Xi'an area, the life cycle cost of the system decreases and CO_2 emissions increase. The minimum water supply temperature is determined as 65 °C for optimal economy and 45 °C for optimal environmental protection.

5.4.2 Equipment price

In the initial investment cost of all equipment in the centralized solar district heating systems, the contributions of the solar collector and the gas boiler are larger. Therefore, the joint multi-objective optimization model developed in this paper was used to simulate the centralized solar district heating system under the condition that the original price of solar collector and gas boiler fluctuated by about 20%. As the pipe diameter design of the centralized heating network is mainly affected by the minimum water supply temperature of the system, only the influence of the price of solar collector and gas boiler on the equipment capacity of the solar heating station is analyzed, as shown in Figure 11.

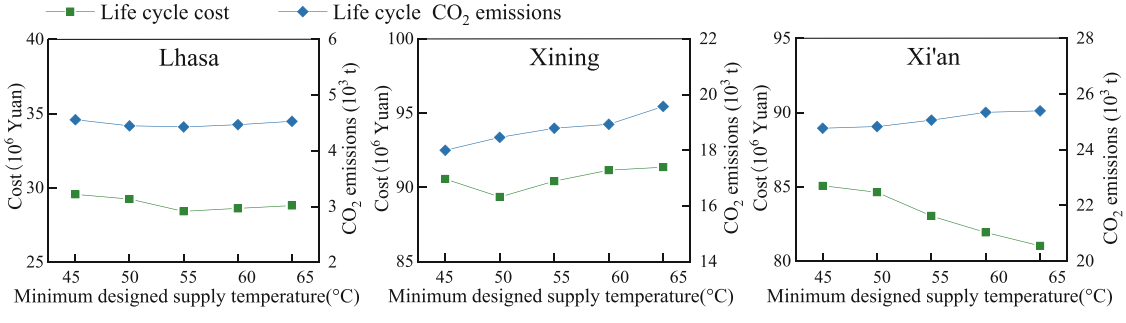

Fig. 10 Comprehensive optimal design results of joint multi-objective optimization for different minimum water supply temperatures

	Price of solar collector	A_{SC} (m^2)	V_S (m^3)	P_{GB} (kW)	Price of gas boiler	A_{SC} (m^2)	V_S (m^3)	P_{GB} (kW)
Lhasa	-20%	11,052	1,819	3,113	-20%	10,507	1,650	3,400
	0	10,629	1,795	3,240	0	10,629	1,795	3,240
	+20%	10,110	1,695	3,454	+20%	10,689	1,934	3,138
Xining	-20%	32,059	6,327	9,274	-20%	30,173	4,678	9,810
	0	30,383	5,163	9,678	0	30,383	5,163	9,678
	+20%	28,512	4,511	10,013	+20%	31,423	5,836	9,437
Xi'an	-20%	22,429	3,359	9,455	-20%	21,000	2,487	9,488
	0	21,778	2,842	9,465	0	21,778	2,842	9,465
	+20%	20,478	2,726	9,478	+20%	20,753	2,791	9,473

Fig. 11 Comprehensive optimal design results obtained by joint multi-objective optimization for different unit prices of solar collector and gas boiler

In Figure 11, with the increase in solar collector price, solar collector area and water tank volume decrease in the comprehensive optimal design of the three cities, and the rated power of the gas boiler increases. With the increase in gas boiler price, collector area and water tank volume of the comprehensive optimal design increase in Lhasa and Xining area, while the rated power of the gas boiler decreases. However, Xi'an exhibits lower sensitivity for gas boiler price and no clear trend of equipment capacity change. Compared with the gas boiler price, the solar collector price has a greater impact on the optimization results of the system. When the unit price of the solar collector increases by 20%, the solar collector areas in Lhasa, Xining, and Xi'an decrease on average by 4.36%, 5.70%, and 4.44%, respectively, the water tank volumes decrease by 3.45%, 15.52%, and 9.74%, respectively, and the rated power of the gas boilers increases on average by 5.34%, 3.91%, and 0.13%, respectively.

6 Conclusions

In this paper, a joint multi-objective optimization model of equipment capacity and pipe diameter of a centralized solar district heating system is developed, and a case analysis is conducted for Lhasa, Xining, and Xi'an with different levels of solar energy resource abundance. The following conclusions are drawn.

(1) Compared with the respective optimization design of the solar heating station and the centralized heating network, the system designed by adopting the joint multi-objective optimization model of a centralized solar district heating system developed in this paper is more reasonable and can achieve higher environmental protection at a lower economic cost. In Lhasa, Xining, and Xi'an, the system life cycle costs decrease by 12.26%, 7.59%, and 3.21%, respectively, and the system life cycle CO_2 emissions decrease by 12.40%, 11.12%, and 11.07%, respectively.

(2) Considering the economy and environmental protection of the centralized solar district heating system, the design value of the solar fraction of the system in Lhasa should be between 50% and 99%, and the optimal value is 90%. In Xining, the solar fraction is between 30% and 93%, and the optimal value is 70%. In Xi'an, the solar fraction lies between 20% and 66%, and its optimal value is determined as 31%.

(3) The minimum water supply temperatures of the centralized solar district heating system optimized for economy or environmental protection are both 55 °C in Lhasa, 50 °C and 45 °C in Xining, and 65 °C and 45 °C in Xi'an.

(4) Compared with the price of the gas boiler, the unit price of the solar collector has a greater impact on the equipment capacity of the solar heating station in the joint multi-objective optimization results of the system. When the unit price of the solar collector increases by 20%, the solar collector area and water tank volume of the system in the Xining area decrease the most, by 5.70% and 15.52%, respectively. The increase in the rated power of the gas boiler of 5.34% in Lhasa is the largest among the three investigated cities.

In this study, the configuration of the solar collector array and dynamic price of solar collectors were not taken into full consideration in the optimization of the centralized solar district heating system. These would be considered in future studies.

Acknowledgements

This research was supported by the National Natural Science Foundation of China (52008328), National Key Research and Development Project (2018YFD1100202), the Science and Technology Department of Shaanxi Province (2020SF-393, 2018ZDCXL-SF-03-04), and the State Key Laboratory of Green Building in Western China (LSZZ202009).

References

Ayele GT, Haurant P, Laumert B, et al. (2018). An extended energy hub approach for load flow analysis of highly coupled district energy networks: Illustration with electricity and heating. *Applied Energy*, 212: 850–867.

BERC (2020). Research Report on the Annual Development of Building Energy Efficiency in China 2020. Building Energy Research Center of Tsinghua University (BERC). Beijing: China Architecture and Building Press. (in Chinese)

Carotenuto A, Figaj RD, Vanoli L (2017). A novel solar-geothermal district heating, cooling and domestic hot water system: Dynamic simulation and energy-economic analysis. *Energy*, 141: 2652–2669.

Chen Y, Liu Y, Wang D, et al. (2020). Performance and optimization of a novel solar-driven liquid desiccant air conditioning system suitable for extremely hot and humid climates. *Energy Conversion and Management*, 215: 112899.

Ding Z, Liu S, Luo L, et al. (2020). A building information modeling-based carbon emission measurement system for prefabricated residential buildings during the materialization phase. *Journal of Cleaner Production*, 264: 121728.

Dobersek D, Goricanec D (2009). Optimisation of tree path pipe network with nonlinear optimisation method. *Applied Thermal Engineering*, 29: 1584–1591.

Dorotić H, Pukšec T, Duić N (2019). Economical, environmental and exergetic multi-objective optimization of district heating systems on hourly level for a whole year. *Applied Energy*, 251: 113394.

Evins R (2013). A review of computational optimisation methods applied to sustainable building design. *Renewable and Sustainable Energy Reviews*, 22: 230–245.

He Z, Zhu D (2009). Technical Handbook for Solar Heat Supply & Space Heating. Beijing: Chemical Industry Press. (in Chinese)

Huang J, Xu Y (2016). The development status and trend of solar district heating in Europe. *Construction Science and Technology*, 2016(23): 63–69. (in Chinese)

Huang J, Fan J, Furbo S, et al. (2019a). Economic analysis and optimization of combined solar district heating technologies and systems. *Energy*, 186: 115886.

Huang J, Fan J, Furbo S, et al. (2019b). Economic analysis and optimization of household solar heating technologies and systems. *Sustainable Energy Technologies and Assessments*, 36: 100532.

Klein SA, Beckman WA, Duffie JA (1976). A design procedure for solar heating systems. *Solar Energy*, 18: 113–127.

Klein SA, Beckman WA (1979). A general design method for closed-loop solar energy systems. *Solar Energy*, 22: 269–282.

Ko MJ (2015). Analysis and optimization design of a solar water heating system based on life cycle cost using a genetic algorithm. *Energies*, 8: 11380–11403.

Kubiński K, Szabłowski Ł (2020). Dynamic model of solar heating plant with seasonal thermal energy storage. *Renewable Energy*, 145: 2025–2033.

Li Y, Liao S, Rao Z, et al. (2014). A dynamic assessment based feasibility study of concentrating solar power in China. *Renewable Energy*, 69: 34–42.

Liu Y, Zhou W, Luo X, et al. (2021). Design and operation optimization of multi-source complementary heating system based on air source heat pump in Tibetan area of western Sichuan, China. *Energy and Buildings*, 242: 110979.

Long T, Qiao Z, Wang M, et al. (2020). Performance analysis and optimization of a solar-air source heat pump heating system in Tibet, China. *Energy and Buildings*, 220: 110084.

Lund H, Werner S, Wiltshire R, et al. (2014). 4th Generation District Heating (4GDH): Integrating smart thermal grids into future sustainable energy systems. *Energy*, 68: 1–11.

Luo X, Liu Y, Liu J, et al. (2020). Energy scheduling for a three-level integrated energy system based on energy hub models: A hierarchical Stackelberg game approach. *Sustainable Cities and Society*, 52: 101814.

Luo X, Liu Y, Feng P, et al. (2021). Optimization of a solar-based integrated energy system considering interaction between generation, network, and demand side. *Applied Energy*, 294: 116931.

Luo X, Sun Y, Liu X, et al. (2022a). Course timetable optimization for a university teaching building considering the building energy efficiency and time-varying thermal perception of students. *Building and Environment*, 219: 109175.

Luo X, Shi W, Jiang Y, et al. (2022b). Distributed peer-to-peer energy trading based on game theory in a community microgrid considering ownership complexity of distributed energy resources. *Journal of Cleaner Production*, 351: 131573.

Mertz T, Serra S, Henon A, et al. (2016). A MINLP optimization of the configuration and the design of a district heating network: Academic study cases. *Energy*, 117: 450–464.

Miedaner O, Pauschinger T (2012). Solar District Heating Guidelines: Categories of solar district heating systems. Available at https://www.solar-district-heating.eu/wp-content/uploads/2018/06/SDH-WP3_FS-6-1_Categories_version2.pdf

MOHURD (2004). JGJ 142-2004: Technical Specification for Floor Radiant Heating. Ministry of Housing and Urban-Rural Development of China (MOHURD). Beijing: China Architecture and Building Press. (in Chinese)

MOHURD (2010). CJJ 34-2010: Design Code for City Heating Network. Ministry of Housing and Urban-Rural Development of China (MOHURD). Beijing: China Architecture and Building Press. (in Chinese)

MOHURD (2015). GB 50189-2015: Design standard for energy efficiency of public buildings. Ministry of Housing and Urban-Rural Development of China (MOHURD). Beijing: China Architecture and Building Press. (in Chinese)

MOHURD (2018). JGJ 26-2018: Design Standard for Energy Efficiency of Residential Buildings in Severe Cold and Cold Zones. Ministry of Housing and Urban-Rural Development of China (MOHURD). Beijing: China Architecture and Building Press. (in Chinese)

MOHURD (2019). GB 50495-2019: Technical Standard for Solar Heating System. Ministry of Housing and Urban-Rural Development of China (MOHURD). Beijing: China Architecture and Building Press. (in Chinese)

National Energy Administration of China (2017). Clean Heating Plan in North China in Winter (2017– 2021). (in Chinese)

Pirouti M, Bagdanavicius A, Ekanayake J, et al. (2013). Energy consumption and economic analyses of a district heating network. *Energy*, 57: 149–159.

Qiu G, Yu S, Cai W (2021). A novel heating strategy and its optimization of a solar heating system for a commercial building in term of economy. *Energy*, 221: 119773.

Ren F, Wang J, Zhu S, et al. (2019). Multi-objective optimization of combined cooling, heating and power system integrated with solar and geothermal energies. *Energy Conversion and Management*, 197: 111866.

Shah SK, Lu A, Rismanchi B (2020). Multi-objective optimisation of a seasonal solar thermal energy storage system for space heating in cold climate. *Applied Energy*, 268: 115047.

State Grid of China (2022). State Grid Online Business Hall. State Grid Corporation of China. Available at http://www.sgcc.com.cn/ywlm/index.shtml

van der Heijde B, Vandermeulen A, Salenbien R, et al. (2019). Integrated optimal design and control of fourth generation district heating networks with thermal energy storage. *Energies*, 12: 2766.

von Rhein J, Henze GP, Long N, et al. (2019). Development of a topology analysis tool for fifth-generation district heating and cooling networks. *Energy Conversion and Management*, 196: 705–716.

Wang D, Liu Y (2010). Temperature stratification studying of heat storage tank. *Building Energy and Environment*, 29(1): 16–19. (in Chinese)

Wang H, Duanmu L, Li X, et al. (2017). Optimizing the district heating primary network from the perspective of economic-specific pressure loss. *Energies*, 10: 1095.

Wang H, Wang H, Zhou H, et al. (2018). Modeling and optimization for hydraulic performance design in multi-source district heating with fluctuating renewables. *Energy Conversion and Management*, 156: 113–129.

Wang W (2017). Evaluation on investment risk of incremental power distribution network based on full life cycle cost and benefit model. *Guangdong Electric Power*, 9(30): 45–51. (in Chinese)

Wang Y, Wang X, Yu H, et al. (2019). Optimal design of integrated energy system considering economics, autonomy and carbon emissions. *Journal of Cleaner Production*, 225: 563–578.

Weiss W, Spörk-Dür M (2018). Solar heat worldwide. Global market development and trends in 2017. Detailed market figures 2016. Gleisdorf, Austria: AEE—Institute for Sustainable Technologies.

Winterscheid C, Dalenbäck JO, Holler S (2017). Integration of solar thermal systems in existing district heating systems. *Energy*, 137: 579–585.

Zhang R, Wang D, Liu Y, et al. (2021). Economic optimization of auxiliary heat source for centralized solar district heating system in Tibetan Plateau, China. *Energy Conversion and Management*, 243: 114385.

Zhou D, Ding H, Wang Q, et al. (2021). Literature review on renewable energy development and China's roadmap. *Frontiers of Engineering Management*, 8: 212–222.

Zhou Z, Liu J, Zeng H, et al. (2022). Carbon performance evaluation model from the perspective of circular economy—The case of Chinese thermal power enterprise. *Frontiers of Engineering Management*, 9: 297–311.